Supporting Online Material for

Radar Imaging of Binary Near-Earth Asteroid (66391) 1999 KW4

Steven. J. Ostro,[*] Jean-Luc Margot, Lance A. M. Benner, Jon D. Giorgini, Daniel J. Scheeres, Eugene G. Fahnestock, Stephen B. Broschart, Julie Bellerose, Michael C. Nolan, Christopher Magri, Petr Pravec, Petr Scheirich, Randy Rose, Raymond F. Jurgens, Eric M. De Jong, Shigeru Suzuki

*To whom correspondence should be addressed. E-mail: ostro@reason.jpl.nasa.gov

This PDF file includes:

> Materials and Methods
> Figs. S1 to S4
> Tables S1 to S4
> References

Supplementary Online Material

for

Radar Imaging of
Near-Earth Binary Asteroid (66391) 1999 KW4

Steven. J. Ostro, Jean-Luc Margot, Lance A. M. Benner, Jon D. Giorgini, Daniel J. Scheeres, Eugene G. Fahnestock, Stephen B. Broschart, Julie Bellerose, Michael C. Nolan, Christopher Magri, Petr Pravec, Petr Scheirich, Randy Rose, Raymond F. Jurgens, Eric M. De Jong, and Shigeru Suzuki

1 Methods

1.1 Observations, Data Analysis, and Shape Modeling

In a radar experiment, one attempts to remove the Doppler frequency shift introduced by the target's radial motion by tuning the frequency of either the transmitter or the receiver according to an ephemeris, with the goal of ensuring that the frequency corresponding to echoes from the target's center of mass (here the binary system's barycenter, BARY) remains constant in the coordinate system of the acquired data. One also uses that ephemeris to slew the time base for sampling the echoes in order to register sequential samples of echoes from any given range cell on the target. In practice, there will always be a nonzero error in the Doppler-prediction ephemeris, which is equivalent to a nonzero rate of change in the delay-ephemeris's error and hence in the rate of image smearing in delay. Our initial KW4 ephemeris was based on available optical astrometry only. During the course of the experiment we subjectively estimated the location of BARY in our delay-Doppler images and used the resultant radar astrometry to refine the orbit. Table S1 gives the orbit solution used for each imaging sequence. The time for drift in the delay-prediction error to cause smearing by one delay resolution cell was between one and six hours, depending on the date. This is much longer than the time span of any images used in our analysis. Smearing in frequency due to drift in Doppler-prediction error is also negligible.

In most of our observations, we used two receiving channels to record echoes in the same rotational sense of circular polarization as transmitted (the SC sense) as well as in the opposite circular (OC). Backreflections from smooth surfaces are almost entirely in the OC sense, and the SC/OC ratio is a measure of the relative contributions to the echo of multiple reflections and scattering from interfaces with radii of curvature comparable to the wavelength. Hence SC/OC is a measure of near-surface wavelength-scale structural complexity, or "roughness."

Beta's motion with respect to the system barycenter is very much faster than Alpha's, so many of the data frames we constructed for Beta are shorter sums and hence slightly weaker than those for Alpha. In our inversion, image frames are organized into sets, and for each set we estimate coefficients of a polynomial that describes the delay-Doppler motion of the component's

COM in that set's frames. We limited the number and the time span of frames in any set in order to ensure that the polynomial can accommodate the object's frame-to-frame translational motion. Our modeling used 121 images for Alpha and 265 for Beta.

Our SHAPE inversion software minimizes an objective function that consists of the weighted sum of (i) the squared residuals between delay-Doppler image pixels and the corresponding values predicted by the physical model, and (ii) penalty functions whose weights can be adjusted to suppress physical attributes that are not required by the data. We experimented with dynamical penalty functions that force uniform rotation or uniform density and structural functions that suppress concavities or topographic roughness, aiming to optimize the trade-off between allowing characteristics needed to match the images and suppressing characteristics that are not geophysically plausible.

Table S1. Observations. For sequences providing useful delay-Doppler resolution of echoes, we give the earliest receive start and the latest stop times, the number of transmit-receive cycles (runs), the number of looks (Fourier transforms) used to produce a delay-Doppler image from the run's echoes, an identifier for the JPL orbit solution used to make the prediction ephemerides used during the observations, the time-delay and Doppler-frequency resolution of the data, and the right ascension, declination, and distance of the asteroid at the midpoint of the data acquisition, and the subradar latitude at that midpoint as predicted from our Alpha model. We received echoes simultaneously in the same sense of circular polarization as transmitted (the SC sense) and in the opposite (OC) sense, but our analyses focused almost entirely on the much stronger OC images. Our Alpha shape modeling used images constructed from sums of three runs. Our Beta shape modeling used single-run images for Arecibo and three-run sums for Goldstone.

UTC Date	UTC Start-Stop hhmmss-hhmmss	Runs	Looks	Orbit	Resolution Delay (us)	Resolution Doppler (Hz)	Midpoint RA,DEC (deg)	Midpoint Dist. (AU)	Model Lat. (deg)
GOLDSTONE									
2001 May 21	150144-154932	22	178	R01/50	1.000	3.000	334,-26	0.060	-39
2001 May 22	130640-155957	88	98	R01/52	0.500	2.000	327,-24	0.051	-35
2001 May 23	101828-135429	133	41	R01/54	0.250	1.000	317,-21	0.043	-29
2001 May 24	085550-153512	167	35	R01/56	0.250	1.000	305,-15	0.037	-19
2001 May 25	083816-144529	234	31	R01/56	0.125	1.000	288, -7	0.033	-6
2001 May 26	052008-053530	13	30	R01/56	0.125	1.000	275, 1	0.032	+7
2001 "	074817-075710	8	98	R01/56	1.000	3.000	273, 2	0.033	+8
2001 "	080849-084704	32	31	R01/56	0.125	1.000	272, 2	0.033	+9
2001 "	090125-135939	187	31	R01/58	0.125	1.000	270, 3	0.033	13
2001 May 28	023907-065503	33	40	R01/60	0.250	1.000	244, 17	0.042	33
2001 "	052031-053212	7	148	R01/60	1.000	3.000	234, 21	0.050	33
2001 May 29	054237-103005	151	102	R01/60	0.500	2.000	233, 21	0.052	40
ARECIBO									
2001 May 26	060603-063122	21	3	R01/56	0.100	0.116	274, 1	0.032	8
2001 "	064309-070549	21	2	R01/56	0.100	0.077	274, 1	0.033	8
2001 May 27	041600-042552	9	3	R01/56	0.100	0.116	259, 10	0.035	21
2001 "	043155-044415	11	3	R01/60	0.100	0.116	258, 10	0.035	22
2001 "	044623-061407	61	2	R01/60	0.100	0.070	258, 10	0.035	22
2001 May 28	040219-043444	19	4	R01/60	0.100	0.116	245, 16	0.041	32
2001 "	043940-051605	26	4	R01/60	0.100	0.116	245, 17	0.042	32
2001 "	051738-054109	17	2	R01/60	0.100	0.057	245, 17	0.042	32
2001 May 29	022000-023000	7	4	R01/60	0.100	0.116	235, 20	0.049	38
2001 "	023141-045753	87	4	R01/60	0.100	0.116	234, 21	0.050	39
2002 Jun 1	214721-230822	20	28	R02/50	2.000	0.239	160, 2	0.127	N/A
2002 Jun 2	221018-231419	15	30	R02/50	2.000	0.239	163, 4	0.137	N/A

Table S2. 66391 (1999 KW4) heliocentric orbit. Least-squares estimates (*S1-S4*) of orbit elements for JPL solution number 77 and formal uncertainties are given for epoch 2005-Aug-04.0 (Coordinate Time). The optical data used in the estimate consist of 1683 usable measurements spanning 1998-May-29 to 2005-Aug-02, with post-fit residual mean and root mean square (rms) of (0.143, 0.657) arcseconds. The normalized rms (n-rms) obtained by first dividing each measurement by its assigned uncertainty is 0.657 since all optical data was weighted at 1 arcsecond. For the 31 radar delay measurements used in the estimate (*S4*), post-fit residual mean and rms are (22, 88) ns and n-rms is 0.281. The combined dataset (optical and radar) n-rms is 0.654. Osculating elements are in the ICRF93/J2000 coordinate frame of the DE-405 JPL planetary ephemeris, a quasar-based radio frame aligned within 0.01 arcseconds of the optical FK5/J2000. Angular elements are referred to the ecliptic and mean equinox of J2000.

```
Osculating element                    Value       Post-Fit Std.Dev.

Eccentricity                     0.6883867034 ± 0.0000000258
Perihelion distance              0.2001480484 ± 0.0000000164 AU
Time of perihelion            2453676.5283086650 ± 0.0000142757 Julian day number
                                (2005-Nov-02.02831)

Longitude of ascending node    244.9330159090 ± 0.0000001442 deg
Argument of perihelion         192.5958593259 ± 0.0000018719 deg
Inclination                     38.8905365946 ± 0.0000023616 deg
Semi-major axis                  0.6422962390 ± 0.0000000030 AU
Orbit period                    188.01889472 ± 0.00000132   days
                                (0.514758659 yrs)
```

Table S3. Radar astrometry. Entries report the round-trip time-delay for hypothetical echoes from the (66391) 1999 KW4 system's barycenter at the indicated UTC reception time. The reference point is the intersection of of the azimuth and elevation axes of the Goldstone 70-m antenna (DSS-14). Estimated standards errors for the measurements are based on echo strength and imaging resolution. Residuals are the measurement minus the prediction of the least-squares orbit solution (Table S2) and are a measure of how well the orbit solution fits the data. One microsecond is 150 m of range.

Observation Time		Delay measurement	Residual
Date (UTC)	HH:MN:SC	(microseconds)	(microseconds)
2001-05-28	06:53:25	42205766.1 ± 0.50	-0.044
2001-05-28	06:43:21	42152816.3 ± 0.50	-0.013
2001-05-28	06:28:39	42075785.7 ± 0.50	-0.009
2001-05-28	06:22:36	42044182.4 ± 0.50	-0.033
2001-05-26	13:58:22	33029703.5 ± 0.25	0.015
2001-05-26	13:36:55	32989192.4 ± 0.25	0.030
2001-05-26	13:20:12	32958346.1 ± 0.25	-0.073
2001-05-26	12:58:36	32919456.9 ± 0.25	0.157
2001-05-26	12:35:00	32878247.3 ± 0.25	-0.057
2001-05-26	12:14:50	32844120.4 ± 0.25	-0.153
2001-05-25	12:33:07	32686883.6 ± 0.25	0.050
2001-05-25	12:03:27	32726073.7 ± 0.25	0.161
2001-05-25	11:05:08	32809994.6 ± 0.25	-0.162
2001-05-25	10:27:24	32869183.1 ± 0.25	-0.021
2001-05-25	09:48:49	32933655.3 ± 0.25	0.006
2001-05-25	09:31:15	32964318.4 ± 0.25	0.084
2001-05-25	09:02:53	33015537.6 ± 0.25	0.034
2001-05-25	08:43:18	33052108.0 ± 0.25	-0.061
2001-05-24	14:51:13	36024797.8 ± 0.50	0.094
2001-05-24	14:28:19	36106446.2 ± 0.50	0.140
2001-05-24	10:48:52	36944120.8 ± 0.50	0.179
2001-05-24	10:30:43	37017895.9 ± 0.50	0.104
2001-05-24	10:17:20	37072719.8 ± 0.50	0.044
2001-05-24	09:39:36	37229188.3 ± 0.50	-0.001
2001-05-23	13:52:45	42912799.3 ± 0.50	0.078
2001-05-23	13:25:58	43056887.3 ± 0.50	0.066
2001-05-23	13:04:05	43175424.9 ± 0.50	0.109
2001-05-23	12:37:44	43319123.3 ± 0.50	0.078
2001-05-23	11:47:02	43598549.6 ± 0.50	-0.093
2001-05-23	11:12:46	43789543.9 ± 0.50	-0.024
2001-05-23	10:41:40	43964326.0 ± 0.50	0.010

Table S4. 66391 (1999 KW4) close approaches. This list of planetary encounters less than 0.1 AU terminates at the last Earth encounter prior to the linearized 3-sigma time of close-approach uncertainty (TCA3sg) exceeding 10 days (14400 minutes) or 0.1 AU, whichever occurs first. The span of reliable encounter prediction so-defined is therefore 1179 to 2946, based on the solution #77 data set. Calendar dates after 1582-Oct-15 are reported in the Gregorian Calendar. Prior to that, dates are reported in Julian Calendar. "CA dist" is the highest probability approach distance of the reference trajectory to the given body. "MinDist" and "MaxDist" are the 3-sigma distances from the body at the nominal encounter time. "Vrel" is the nominal relative velocity. Integrations were performed using the DE-405 planetary ephemeris and include relativistic perturbations due to the Sun, planets, and Moon as well as asteroids Ceres, Pallas and Vesta. The limits of predictability for objects having multiple planetary encounters over centuries will normally be affected by additional factors such as radiation pressure, Yarkovsky acceleration, planetary mass uncertainties, and asteroid perturbations. These factors are not included here, since the relevant physical models are imprecisely defined and key parameters are unmeasured.

Date	Body	CA dist AU	MinDist AU	MaxDist AU	Vrel km/s	TCA3Sg min
1179 May 09.07555	Earth	0.022047	0.022043	0.050490	20.746	892.27
1196 May 09.54391	Earth	0.056011	0.031941	0.085159	20.053	1315.2
1197 May 08.30464	Earth	0.061500	0.032322	0.094942	21.816	63.65
1214 May 08.97781	Earth	0.021734	0.021721	0.025775	20.770	252.47
1231 May 10.40120	Earth	0.054403	0.046381	0.062805	20.082	381.92
1232 May 08.23819	Earth	0.063177	0.053585	0.073020	21.867	28.95
1248 May 11.48785	Earth	0.099467	0.095901	0.103060	19.712	233.86
1249 May 08.87115	Earth	0.021612	0.021416	0.022565	20.811	75.43
1266 May 10.19084	Earth	0.050486	0.047410	0.053625	20.138	137.99
1267 May 09.18146	Earth	0.068101	0.064323	0.071908	21.995	19.68
1283 May 12.19660	Earth	0.095205	0.093309	0.097109	19.733	120.75
1284 May 08.72886	Earth	0.022640	0.021915	0.023573	20.902	36.10
1301 May 09.80951	Earth	0.040311	0.038086	0.042597	20.282	91.76
1302 May 09.17720	Earth	0.081166	0.078177	0.084165	22.319	29.34
1318 May 11.61524	Earth	0.083815	0.081642	0.085999	19.808	127.42
1319 May 09.51474	Earth	0.030848	0.028917	0.032896	21.162	26.82
1336 May 09.35853	Earth	0.026842	0.025620	0.028159	20.518	52.67
1353 May 10.94795	Earth	0.068629	0.067277	0.069986	19.942	69.49
1354 May 09.35058	Earth	0.046439	0.044956	0.047935	21.533	4.44
1371 May 10.08675	Earth	0.021077	0.020891	0.021283	20.685	14.30
1388 May 10.62230	Earth	0.061666	0.061227	0.062105	20.020	21.02
1389 May 09.26610	Earth	0.054205	0.053705	0.054707	21.722	0.34
1406 May 09.96124	Earth	0.020106	0.020071	0.020143	20.727	3.98
1423 May 11.52538	Earth	0.061274	0.061121	0.061428	20.029	7.26
1424 May 09.19781	Earth	0.054394	0.054218	0.054571	21.744	0.21
1441 May 09.92572	Earth	0.020588	0.020554	0.020622	20.680	2.13
1458 May 11.72832	Earth	0.069746	0.069627	0.069865	19.946	6.07
1459 May 10.13505	Earth	0.044128	0.043994	0.044263	21.533	0.39
1476 May 10.05066	Earth	0.026986	0.026893	0.027080	20.498	3.48
1477 May 09.97711	Earth	0.098049	0.097901	0.098198	22.793	2.31
1493 May 12.29089	Earth	0.086961	0.086863	0.087058	19.806	5.72
1494 May 10.15943	Earth	0.026200	0.026117	0.026283	21.134	1.27
1511 May 11.36919	Earth	0.042419	0.042341	0.042497	20.247	3.02
1512 May 09.72848	Earth	0.076773	0.076677	0.076869	22.286	0.89
1528 May 12.60783	Earth	0.096773	0.096739	0.096807	19.744	2.11
1529 May 10.18370	Earth	0.019670	0.019656	0.019683	20.944	0.58
1546 May 11.46498	Earth	0.049105	0.049077	0.049133	20.166	1.15
1547 May 10.61908	Earth	0.068736	0.068702	0.068770	22.107	0.23
1563 May 13.54868	Earth	0.097679	0.097665	0.097693	19.736	0.90
1564 May 10.11598	Earth	0.019096	0.019091	0.019101	20.940	0.26

```
1581 May 11.22287   Earth   0.043412 0.043392 0.043432   20.251   0.78
1582 May 10.59589   Earth   0.076023 0.075997 0.076048   22.286   0.24
1598 May 23.11460   Earth   0.089755 0.089735 0.089774   19.779   1.14
1599 May 20.95033   Earth   0.024061 0.024044 0.024077   21.122   0.27
1616 May 20.74730   Earth   0.027484 0.027467 0.027501   20.514   0.60
1617 May 20.72113   Earth   0.097311 0.097286 0.097336   22.814   0.39
1633 May 22.32459   Earth   0.071458 0.071443 0.071474   19.927   0.77
1634 May 20.77401   Earth   0.042534 0.042517 0.042551   21.555   0.05
1651 May 21.44338   Earth   0.018577 0.018575 0.018579   20.742   0.13
1668 May 21.96354   Earth   0.063379 0.063377 0.063381   20.016   0.08
1669 May 20.69333   Earth   0.051426 0.051425 0.051428   21.758   0.01
1686 May 21.35126   Earth   0.017836 0.017834 0.017837   20.762   0.05
1703 May 24.06685   Earth   0.069214 0.069203 0.069225   19.966   0.53
1704 May 21.61133   Earth   0.044340 0.044327 0.044353   21.610   0.00
1721 May 22.45039   Earth   0.024462 0.024449 0.024475   20.574   0.41
1722 May 22.54670   Earth   0.099449 0.099429 0.099469   22.921   0.35
1738 May 24.64535   Earth   0.087441 0.087426 0.087457   19.818   0.89
1739 May 22.61484   Earth   0.024432 0.024418 0.024446   21.177   0.16
1756 May 22.77512   Earth   0.041850 0.041836 0.041864   20.288   0.50
1757 May 22.25590   Earth   0.076809 0.076792 0.076825   22.386   0.19
1773 May 24.97050   Earth   0.097710 0.097704 0.097717   19.754   0.37
1774 May 22.63111   Earth   0.017126 0.017123 0.017128   20.978   0.09
1791 May 23.79950   Earth   0.046031 0.046023 0.046040   20.229   0.31
1792 May 22.15302   Earth   0.072138 0.072128 0.072149   22.286   0.11
1808 May 25.76078   Earth   0.095006 0.094998 0.095013   19.773   0.45
1809 May 23.51696   Earth   0.018693 0.018688 0.018698   21.063   0.10
1826 May 24.37391   Earth   0.031633 0.031620 0.031645   20.438   0.38
1827 May 24.24894   Earth   0.090718 0.090702 0.090734   22.738   0.25
1843 May 25.94937   Earth   0.076171 0.076159 0.076182   19.916   0.59
1844 May 23.32534   Earth   0.037006 0.036993 0.037019   21.515   0.03
1861 May 23.96922   Earth   0.016873 0.016870 0.016876   20.749   0.12
1878 May 25.47751   Earth   0.064572 0.064565 0.064579   20.027   0.33
1879 May 24.25222   Earth   0.049860 0.049852 0.049869   21.812   0.03
1896 May 23.87767   Earth   0.016301 0.016297 0.016304   20.770   0.12
1913 May 26.71622   Earth   0.074528 0.074515 0.074541   19.928   0.62
1914 May 25.18222   Earth   0.037602 0.037588 0.037617   21.555   0.03
1931 May 26.08070   Earth   0.029668 0.029654 0.029681   20.493   0.39
1932 May 25.06212   Earth   0.091172 0.091156 0.091189   22.771   0.27
1948 May 27.37013   Earth   0.094563 0.094555 0.094570   19.768   0.43
1949 May 25.21584   Earth   0.017243 0.017238 0.017248   21.095   0.09
1966 May 26.32598   Earth   0.044292 0.044286 0.044298   20.286   0.21
1967 May 25.83143   Earth   0.073746 0.073739 0.073753   22.364   0.08
1983 May 28.36220   Earth   0.096900 0.096898 0.096902   19.753   0.12
1984 May 25.14796   Earth   0.016078 0.016077 0.016079   21.071   0.02
2001 May 25.97992   Earth   0.032332 0.032332 0.032332   20.469   0.00
2002 May 25.90998   Earth   0.088928 0.088928 0.088928   22.743   0.00
2018 May 27.55782   Earth   0.078186 0.078184 0.078188   19.900   0.09
2019 May 25.96154   Earth   0.034633 0.034631 0.034635   21.513   0.00
2036 May 25.57165   Earth   0.015534 0.015533 0.015536   20.798   0.06
2053 May 27.13010   Earth   0.067837 0.067830 0.067844   20.007   0.30
2054 May 25.88679   Earth   0.045674 0.045666 0.045682   21.760   0.02
2071 May 26.53526   Earth   0.017531 0.017525 0.017537   20.740   0.17
2088 May 27.67952   Earth   0.086560 0.086551 0.086569   19.844   0.47
2089 May 25.84408   Earth   0.023838 0.023829 0.023847   21.299   0.06
2106 May 27.88172   Earth   0.039420 0.039416 0.039424   20.363   0.13
2107 May 27.59663   Earth   0.079023 0.079018 0.079027   22.557   0.06
2123 May 30.03044   Earth   0.098019 0.098017 0.098022   19.767   0.13
2124 May 26.84355   Earth   0.014109 0.014107 0.014110   21.071   0.03
2141 May 27.75773   Earth   0.037573 0.037558 0.037587   20.387   0.43
2142 May 27.55826   Earth   0.082394 0.082376 0.082412   22.649   0.26
2158 May 29.45181   Earth   0.085471 0.085453 0.085489   19.865   0.93
2159 May 27.68042   Earth   0.026224 0.026204 0.026243   21.382   0.09
2176 May 27.27578   Earth   0.015938 0.015930 0.015946   20.762   0.19
2193 May 28.84911   Earth   0.070153 0.070151 0.070154   20.008   0.05
```

```
2194 May 27.59310  Earth  0.043095 0.043094 0.043096  21.762  0.00
2211 May 29.22565  Earth  0.017669 0.017662 0.017676  20.724  0.17
2228 May 30.39549  Earth  0.088638 0.088626 0.088650  19.842  0.65
2229 May 28.55078  Earth  0.021159 0.021146 0.021172  21.309  0.09
2246 May 29.53398  Earth  0.039168 0.039162 0.039175  20.373  0.20
2247 May 29.33395  Earth  0.079479 0.079471 0.079486  22.598  0.10
2263 May 31.65027  Earth  0.097815 0.097812 0.097818  19.770  0.16
2264 May 28.53070  Earth  0.013303 0.013301 0.013306  21.139  0.04
2281 May 29.24394  Earth  0.028299 0.028283 0.028316  20.550  0.41
2282 May 29.42946  Earth  0.093477 0.093457 0.093497  22.945  0.37
2298 May 30.76421  Earth  0.076098 0.076080 0.076115  19.942  0.82
2299 May 29.37614  Earth  0.036863 0.036842 0.036883  21.668  0.02
2316 May 29.90477  Earth  0.012022 0.012016 0.012028  20.882  0.16
2333 May 31.62815  Earth  0.074732 0.074717 0.074747  19.958  0.70
2334 May 30.29741  Earth  0.037184 0.037166 0.037202  21.679  0.02
2351 May 31.05570  Earth  0.026464 0.026450 0.026477  20.599  0.32
2352 May 30.30248  Earth  0.093705 0.093689 0.093720  22.976  0.28
2368 Jun 01.36354  Earth  0.098067 0.098066 0.098067  19.767  0.01
2369 May 30.29378  Earth  0.012067 0.012067 0.012068  21.140  0.00
2386 May 31.16255  Earth  0.037014 0.036999 0.037029  20.442  0.42
2387 May 31.10246  Earth  0.082484 0.082466 0.082503  22.718  0.30
2403 Jun 01.84824  Earth  0.087012 0.086991 0.087032  19.857  1.03
2404 May 30.15672  Earth  0.024319 0.024296 0.024342  21.422  0.07
2421 May 30.70999  Earth  0.014052 0.014046 0.014058  20.833  0.12
2438 Jun 01.38951  Earth  0.076050 0.076036 0.076063  19.965  0.62
2439 May 31.07499  Earth  0.035779 0.035762 0.035796  21.671  0.02
2456 May 30.77180  Earth  0.023419 0.023392 0.023446  20.656  0.59
2457 May 31.15015  Earth  0.097551 0.097520 0.097583  23.121  0.62
2473 Jun 01.96527  Earth  0.095221 0.095210 0.095232  19.805  0.60
2474 May 31.03854  Earth  0.014035 0.014025 0.014045  21.225  0.09
2491 May 31.80024  Earth  0.030294 0.030276 0.030313  20.543  0.45
2492 May 30.99327  Earth  0.090732 0.090709 0.090756  22.966  0.45
2508 Jun 02.39998  Earth  0.081967 0.081935 0.082000  19.921  1.57
2509 May 31.91688  Earth  0.029910 0.029871 0.029949  21.575  0.00
2526 Jun 01.47935  Earth  0.014090 0.014069 0.014111  20.822  0.38
2543 Jun 03.44398  Earth  0.085720 0.085696 0.085743  19.892  1.19
2544 May 31.84805  Earth  0.024254 0.024223 0.024284  21.475  0.06
2561 Jun 01.66910  Earth  0.032616 0.032569 0.032662  20.507  1.14
2562 Jun 01.82124  Earth  0.087088 0.087035 0.087142  22.896  0.96
2578 Jun 03.72591  Earth  0.096035 0.096004 0.096065  19.806  1.63
2579 Jun 01.80914  Earth  0.013507 0.013476 0.013537  21.269  0.22
2596 Jun 01.35817  Earth  0.017316 0.017272 0.017360  20.767  0.80
2613 Jun 03.85609  Earth  0.073067 0.073023 0.073112  20.008  1.92
2614 Jun 02.71867  Earth  0.040163 0.040111 0.040215  21.837  0.21
2631 Jun 03.24248  Earth  0.014081 0.014061 0.014102  20.840  0.35
2648 Jun 04.61765  Earth  0.098142 0.098097 0.098188  19.786  2.48
2649 Jun 02.67043  Earth  0.010044 0.009997 0.010092  21.223  0.42
2666 Jun 03.37970  Earth  0.030099 0.030078 0.030119  20.577  0.45
2667 Jun 03.67905  Earth  0.091032 0.091011 0.091052  23.013  0.41
2683 Jun 04.91382  Earth  0.081026 0.080999 0.081053  19.929  1.31
2684 Jun 02.55200  Earth  0.031689 0.031653 0.031724  21.675  0.06
2701 Jun 04.04443  Earth  0.010416 0.010366 0.010466  20.933  0.78
2718 Jun 06.30072  Earth  0.094816 0.094743 0.094890  19.810  3.80
2719 Jun 04.50092  Earth  0.013306 0.013217 0.013395  21.307  0.49
2736 Jun 04.28967  Earth  0.034767 0.034741 0.034794  20.524  0.66
2737 Jun 04.47287  Earth  0.085420 0.085382 0.085458  22.901  0.66
2753 Jun 06.03268  Earth  0.090220 0.090106 0.090333  19.850  5.78
2754 Jun 04.41034  Earth  0.020584 0.020446 0.020723  21.460  0.28
2771 Jun 04.90272  Earth  0.011601 0.011589 0.011614  20.917  0.19
2788 Jun 05.84252  Earth  0.087315 0.087177 0.087453  19.882  6.61
2789 Jun 04.33157  Earth  0.022616 0.022445 0.022788  21.505  0.15
2806 Jun 05.11823  Earth  0.034217 0.034122 0.034312  20.537  2.21
2807 Jun 05.33314  Earth  0.085748 0.085646 0.085850  22.944  1.95
2823 Jun 07.08240  Earth  0.096810 0.096784 0.096837  19.809  1.57
```

```
2824 Jun 04.27056   Earth   0.012425 0.012386 0.012464   21.312    0.18
2841 Jun 04.70157   Earth   0.007277 0.007260 0.007295   21.002    0.23
2858 Jun 07.00047   Earth   0.096966 0.096865 0.097066   19.820    5.19
2859 Jun 05.19771   Earth   0.010751 0.010631 0.010872   21.294    0.63
2876 Jun 04.82877   Earth   0.026435 0.026094 0.026775   20.655    6.66
2877 Jun 05.33953   Earth   0.095580 0.095178 0.095982   23.215    8.56
2893 Jun 06.33726   Earth   0.079920 0.079505 0.080335   19.977   18.37
2894 Jun 05.11888   Earth   0.033135 0.032639 0.033631   21.759    1.69
2911 Jun 06.57391   Earth   0.011006 0.010804 0.011209   20.925    2.68
2929 Jun 06.08785   Earth   0.003163 0.002875 0.003830   21.185    9.34
2929 Jun 06.26860   Moon    0.002655 0.002654 0.002943   20.802   14.08
2946 Jun 06.46567   Earth   0.007295 0.002755 0.066539   21.007  626.69
```
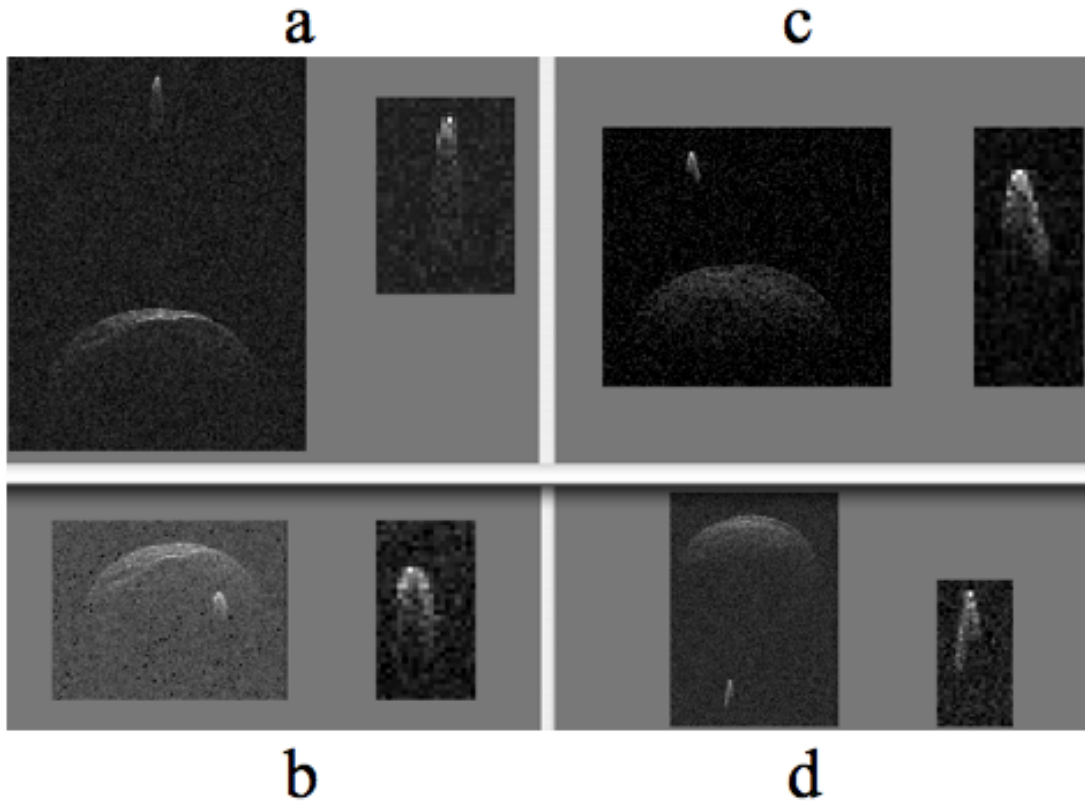
Fig. S1

Single-run Arecibo images with close-ups of Beta. Two images are near epochs determined from the shape modeling to have the components' COMs aligned in Doppler (a) or range (b), and show Beta's limbs to have similar extents. The other two are near epochs midway between conjunctions and show Beta's limbs to have very different extents. Range increases downward and Doppler increases to the right. Rotation and Beta's orbital motion are counterclockwise. The eight pictures have different delay-Doppler dimensions, but in each the delay resolution is 100 ns (15 m in range) and the Doppler resolution is 0.116 Hz (7.3 mm s^{-1}). The UT start-receive epoch, ddhhmmss = 29024153, of (a) is 0.7 minutes before Doppler conjunction. He epoch of (b), 28043409, is 1.3 min before range conjunction. The other images' epochs are (c) 26061359 and (d) 27043309.
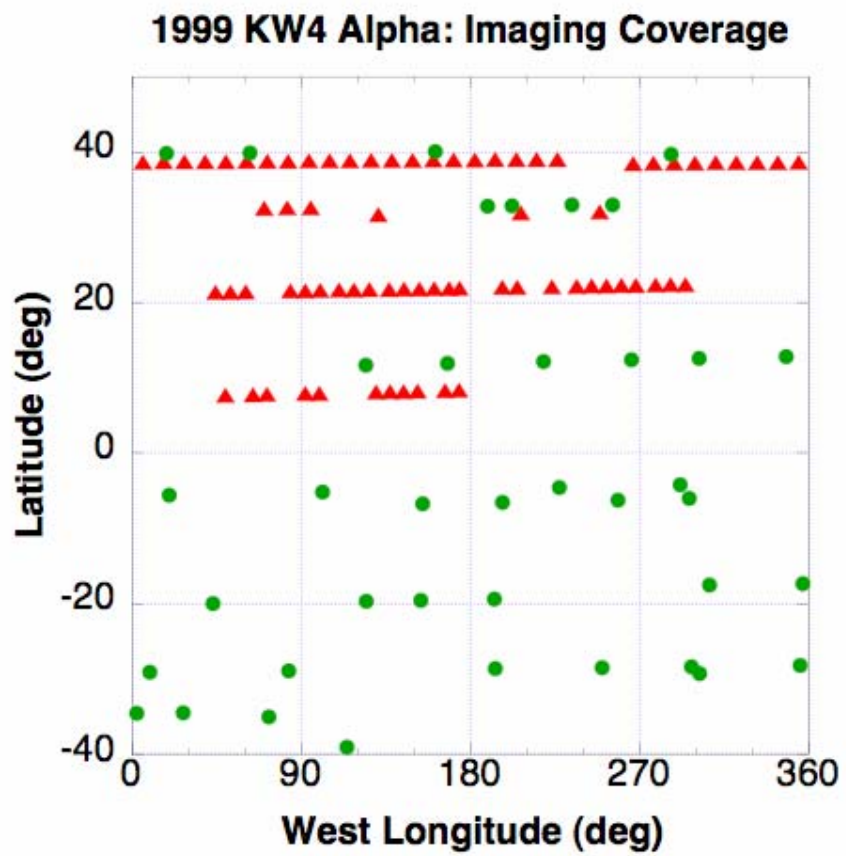
Fig. S2

Orientational coverage provided by Arecibo (red triangles) and Goldstone (green circles) images used in modeling of Alpha, using the estimated pole direction (Table 2). Beta imaging coverage was slightly more extensive.
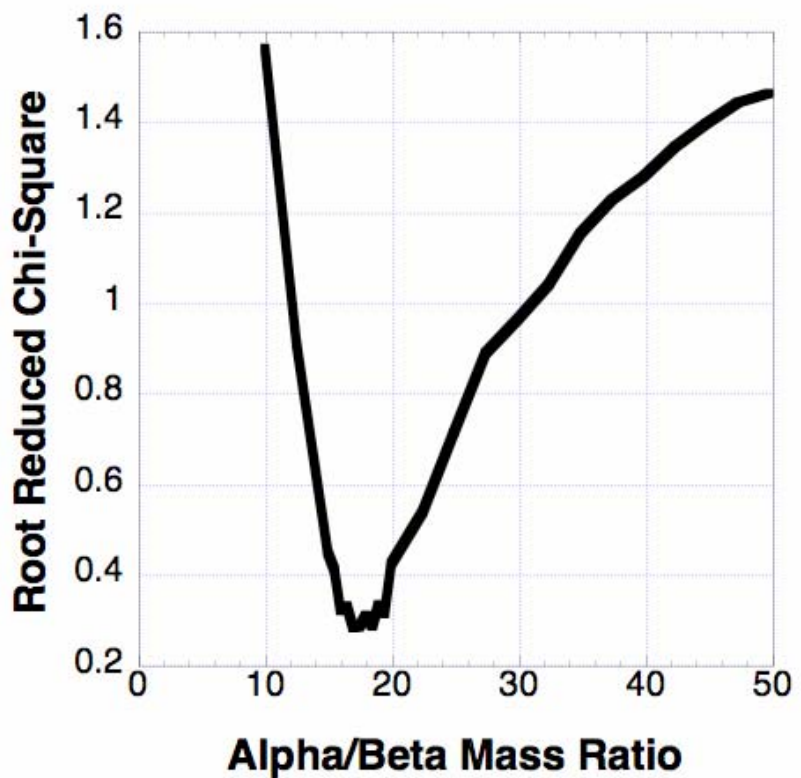
Fig. S3

Root-reduced chi-square for the barycenter delay residuals (Table S3) in the heliocentric orbit estimate (Table S2), as a function of the assumed Alpha/Beta mass ratio.
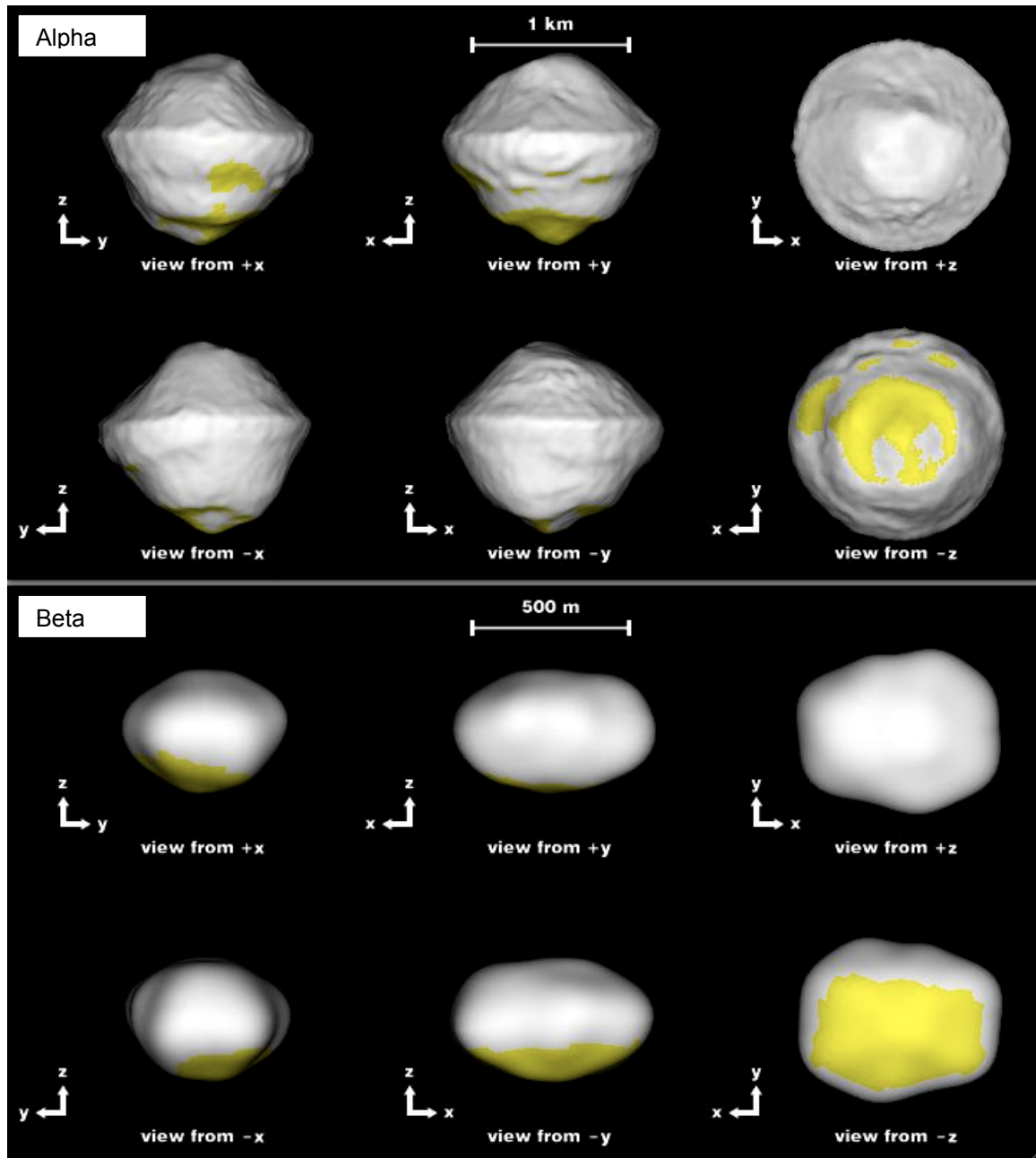
Fig. S4

Principal-axis views of the Alpha (top) and Beta shape models. Yellow-shaded regions were not viewed in Arecibo images at incidence angles less than 70 degrees. Since their modeling relied heavily or entirely on Goldstone images, which are weaker than the Arecibo images, the accuracy of our reconstruction probably is lower there than for the rest of the model.

References

S1. C. L. Lawson, R. Hanson, *Solving Least Squares Problems*, SIAM Classics in Applied Mathematics, vol. 15 (Society for Industrial and Applied Mathematics, Philadelphia, PA, 1995).

S2. G. J. Bierman, *Factorization Methods for Discrete Sequential Estimation* (Academic Press, New York, 1977).

S3. J. D. Giorgini et al., *Science* **296**, 132 (2002).

S4. http://ssd.jpl.nasa.gov/?grp=ast&fmt=html&radar=